AIChE WILEY InterScience DISCOVER SOMETHING GREAT

PROCESS SYSTEMS ENGINEERING

Characterization of Dynamical Emulsification Process in Concentrated Conditions

Christophe Baravian, Julien Mougel, and François Caton
Nancy University, Laboratoire d'Energétique et de Mécanique Théorique et Appliquée, CNRS UMR 7563, 2, avenue de la forêt de Haye BP 160, 54504 Vandoeuvre Cedex, France

Alain Durand
National Polytechnique Institut of Lorraine, Laboratoire de Chimie Physique Macromoléculaire CNRS UMR 7568, 1 Rue Grandville BP 451, 54001 Nancy Cedex, France

DOI 10.1002/aic.11229
Published online June 19, 2007 in Wiley InterScience (www.interscience.wiley.com).

Emulsification at constant shear rate in concentrated conditions (50% in volume fraction) is investigated experimentally by measuring simultaneously the droplet size and the global shear stress using a specially designed rheo-optical "Steady Light Transport" apparatus. The capillary number is varied by changing the continuous phase viscosity, corresponding to disperse to continuous phase viscosity ratios between 0.02 and 2. We show that when the capillary number is large enough (>0.35), emulsification occurs. At constant shear rate, this time-dependant process can be separated into four steps: (1) flow start-up, (2) premix formation, (3) a progressive reduction in droplet size, associated with an increase in shear stress, (4) changes in droplet size and shear stress stop at a well-defined emulsification time. Step (3), called dynamical emulsification, is fully controlled by the critical capillary number and the mechanism of drop size reduction stops when viscous dissipation dominates the droplet elongation and break-up mechanism. This approach accurately describes both the variation in shear stress with droplet size during Stage (3) and the final state of the emulsion in terms of droplet size and viscosity. © 2007 American Institute of Chemical Engineers *AIChE J,* 53: 1994–2000, 2007

Keywords: rheology, mixing, interfacial processes, multi-phase flow, particle/count/measurements

Introduction

To disperse one fluid into another immiscible fluid, some mechanical energy (e.g. shear) is used together with a surfactant to produce a dispersion with stable properties (such as final droplet size, polydispersity, and rheology). The nature of the two fluids, the surfactant and the process conditions (shape of the agitator, agitation rate, and duration) all have a critical effect on the properties of the final emulsion (see e.g. Refs. 1–3).

Most of the publications dealing with the transition between the initial phase-separated state and the final dispersion focus on individual droplets deformation or break-up.[4,5] Among those, Taylor's seminal work[4] described the deformation and break-up of a single drop. Under constant shear rate, the initially spherical drop deforms to an ellipsoid (length L and breadth B). For small deformations, Taylor showed theoretically that the deformation $(L - B)/(L + B)$ is mainly given by a capillary number of the form: $\mathrm{Ca} = \dot{\gamma}\eta_c R/\gamma$, where $\dot{\gamma}$ is the applied shear rate, η_c is the con-

Correspondence concerning this article should be addressed to C. Baravian at Christophe.baravian@ensem.inpl-nancy.fr.

tinuous phase viscosity, R is the spherical drop radius and γ is the interfacial tension between the two phases. When Ca increases, the drop elongates, forms a thread, and finally breaks up into smaller drops, defining a critical deformation, or a critical capillary number Ca_{cr} at burst. This critical capillary number corresponds to the minimum shear stress $\sigma = \dot{\gamma}\eta_c$ needed to overcome the Laplace pressure γ/R inside the drop. For simple shear flow, Grace[5] showed that Ca_{cr} depends on the ratio between the dispersed phase viscosity (η_d) and the continuous phase viscosity with a minimum plateau value close to 0.6 when η_d/η_c is between 0.01 and 1. He also showed that the shear should be applied for a certain time t_B to burst the drop, the reduced time $t_B\gamma/(2R\eta_c)$ being an increasing function of η_d/η_c. Finally, Mabille et al.[6] showed that the final radius R is approximately proportional to γ/σ at fixed η_d/η_c for an emulsion.

A major goal of our work is to study the time dependence of emulsification process in concentrated systems (50% in volume fraction) as industrial emulsions are often produced in concentrated situations. Indeed, multiple hydrodynamic interactions between droplets might affect the elongation break-up mechanism, and therefore affect the dynamical emulsification process.

As such concentrated suspensions are highly turbid and produced under fast flows, standard optical methods (e.g. microscopy, Small Angle Light Scattering, Diffusive Wave Spectroscopy) are unable to provide any droplet size measurement. Thus we use a recently developed technique particularly well suited to this problem, called Steady Light Transport (SLT).[7] The simultaneous measurement of changes in droplet size (using SLT) and shear stress allow an experimental investigation of how the mechanical energy provided by a constant shear rate is used to create the dispersion. The volume fraction, the dispersed phase viscosity and interfacial tension are maintained constant in all experiments. To study the influence of the capillary number on the emulsification process, the viscosity of the continuous phase is varied to obtain a range of viscosity ratios $0.02 < \eta_d/\eta_c < 2$.

First, we describe the experimental apparatus, the materials and the experimental protocols. Then, we present the evolution of size and stress during emulsification at constant shear rate and identify the different steps of the emulsification process. The two last sections concern the analysis of the experimental results in the transitory regime as well as the final state of the emulsion.

Experimental Device and Materials

Figure 1 shows the experimental apparatus. There are two parts: a rheometer (AR 1000, TA Instruments) and an optical device. Experiments are performed in a temperature-controlled room at (20 ± 1)°C.

Vane geometry calibration

The measurement geometry used for rheometry is a six-blade vane of radius $R_V = 11$ mm and immersed height $h = 24$ mm. This vane is centred inside a fixed cylinder of inner radius $R_C = 12.3$ mm sealed onto a glass plate. This geometry is known to produce a purely azimutal flow identical to the flow between two effective concentric cylinders (Ref. 8 and included references). Using the protocol described in Ref. 8 and several silicon oils of known viscosity, the following shear stress and shear rate geometrical factors of the vane are obtained: $F_\sigma = 54935\ m^{-3}$ and $F_{\dot{\gamma}} = 9.90$. For all emulsification experiments, the angular velocity Ω is set at 100 rad/s, leading to a shear rate $\dot{\gamma} = \Omega F_{\dot{\gamma}} = 990\ s^{-1}$. The stress is given by $\sigma = \Gamma F_\sigma$, where Γ is the torque. We also checked that except for the water continuous phase, the flow remains stable and laminar.

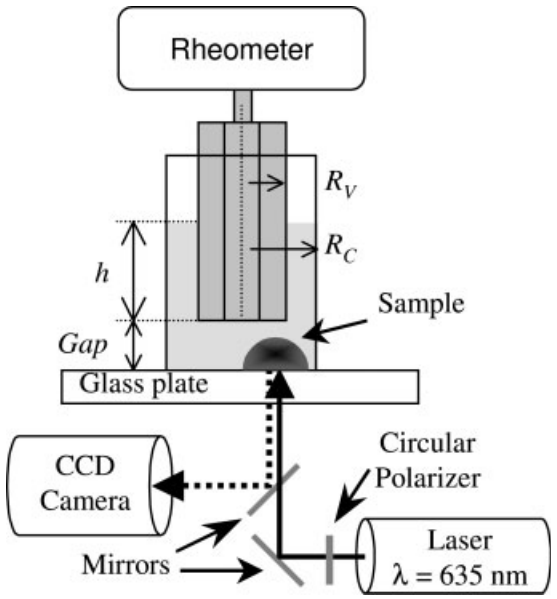

Figure 1. Rheo-optical apparatus.

Optical device

The optical part of the apparatus has already been used to study emulsions.[7,9,10] It consists of a laser diode (wavelength $\lambda = 635$ nm), a circular polarizer to control incident polarisation, a CCD camera as detector and two mirrors (Figure 1). The choice of the radial position of the laser impact at the bottom of the geometry is not arbitrary. It corresponds to the center of the recirculation zone where there is an exchange between the sheared zone and the bottom of the geometry, so that size measurements are representative of the sheared region. The camera records the light backscattered by the sample yielding a $5 \times 5\ mm^2$ image. It represents the backscattered incoherent light transport far from the impact of the laser (the radius of the incident laser spot is 27 μm). Figure 2a shows an example of an experimental angularly averaged radial intensity decrease of light, $I(\rho)$, where ρ is the radial distance from the center of the spot.

Determination of droplet sizes

The spatial intensity decrease measured above is fitted by a steady state radiative transfer model in the diffusion approximation.[7,11,12,13] As this diffusion model only involves a single variable: the transport length l_{tr}, it is thus determined unambiguously (Figure 2a).

In the case of emulsification process, the optical refractive index and volume fraction of droplets remain constant, so a

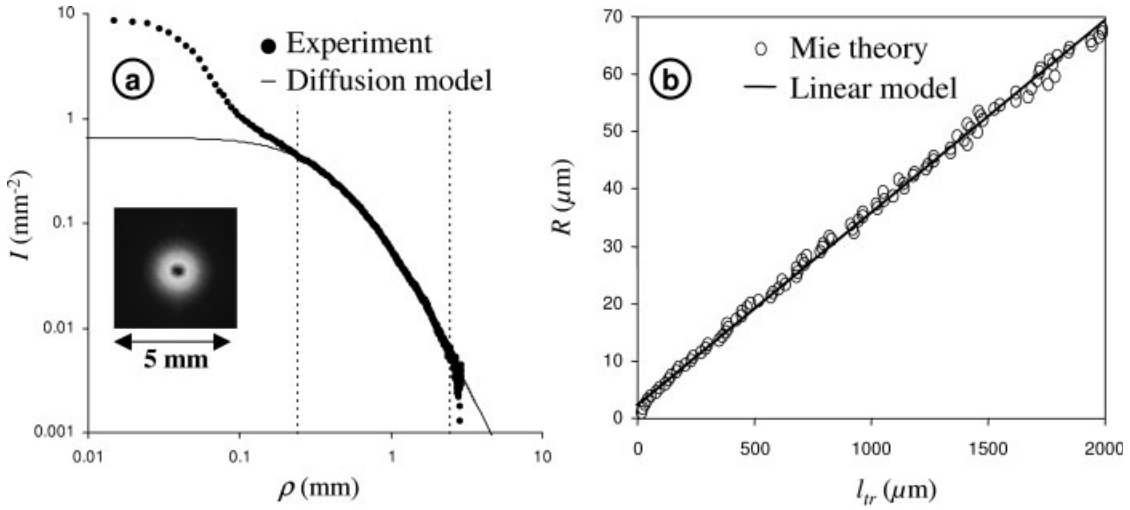

Figure 2. (a) Backscattering spot for the 40.1 mPa s emulsion at t = 810 s and adjustment of the diffusion model to the experimental decrease of the radial distribution of backscattered light, with l_{tr} = 341 μm. (b) Size inversion used from Mie theory.

The continuous line corresponds to Eq. 1.

change of the transport length is only due to a modification of average droplet size.[7,10] From Mie theory, the dependence of the transport length on the size of droplets can be calculated using the optical refractive index of the dispersed phase, and the actual dispersed volume fraction.[7] Figure 2b shows the linear dependence of the droplet radius with the calculated transport length for the present case (hexadecane droplets dispersed in an aqueous phase at 50% in volume fraction). Therefore, the determination of an average radius of droplets from the experimentally determined transport length is straightforward (Figure 2b).

We verified that, in spite of the large volume fraction, the effect of dependent diffusion through position correlation is negligible in the studied droplet size range. Particle size inversion is performed by representing the curve $R(l_{tr})$ by a straight line (Figure 2b). The best least squares fit gives:

$$R = 0.033 l_{tr} + 2.7, \quad (1)$$

where R and l_{tr} are in μm. The absolute error in particle size determination is typically of the order of one μm for the present study (7 μm $< R <$ 70 μm). The size measured by this technique corresponds to the average droplet size in volume,[7] and a detailed discussion can be found in Ref. 13.

Experiment procedure and materials

Initially, the aqueous and the oil phases are superposed in the cylinder. We avoid mixing them, so that the initial state is reproducible. At t = 0, constant agitation (Ω = 100 rad/s, i.e. $\dot{\gamma} = 990 s^{-1}$) is started. During the three-hour experiment, the rheometer measures the stress and the light transport device records one image every 90 s. At the end of the experiment, the final emulsion is collected and, after extensive dilution, (about 15 emulsion drops in half a litre of water), its size distribution is determined by small angle light scattering (SALS) in a Malvern Mastersizer X, using Malvern's inversion program. It has been independently verified using Dynamical Light Scattering that the average droplet size remains constant upon dilution.

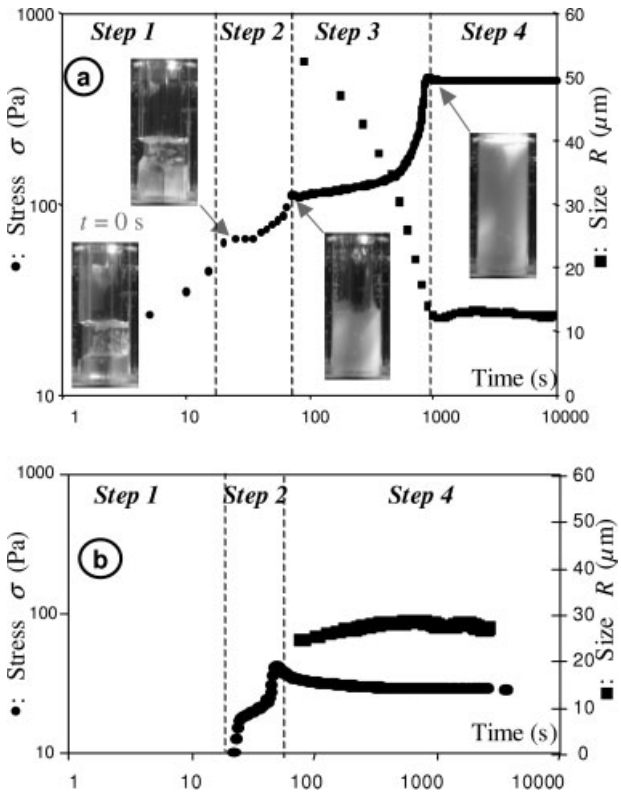

Figure 3. Steps in the emulsification process.

(a) Type 1 emulsion with existence of Step 3 (dynamical emulsification). Continuous phase viscosity = 40.1 mPa s. (b) Type 2 emulsion with no Step 3. Continuous phase viscosity = 6 mPa s.

The dispersed oil phase is hexadecane (99% purum, Sigma-Aldrich) with a viscosity of $\eta_d = 3.45 \pm 0.1$ mPa s. We prepared continuous phases with viscosities in the range of 1 mPas $< \eta_c <$ 155 mPas. The first aqueous phase prepared contains 20 g/L of surfactant dissolved in water. The surfactant is an amphiphilic polysaccharide: dextran (T40, 4×10^4 g/mol supplied by Pharmacia) modified in the following way. The polymer is made interfacially active by randomly grafting of hexyl groups onto 20% of the sugar monomers.[14] The viscosity of this aqueous phase is $\eta_c = 1.7 \pm 0.1$ mPa s. The interfacial tension is the same for all samples: $\gamma = 0.01 \pm 10^{-3}$ N/m. The modified polymer concentration remains constant in all experiments and is assumed to play the same role for all experiments.[15]

Increasing viscosities are obtained by adding increasing amounts of non-modified dextran (T2000, 2×10^6 g/mol supplied by Pharmacia), resulting in four continuous phases at $\eta_c = 6$, 12, 20.6, and 29 mPa s.

To explore a larger range of continuous phase viscosity, we use another polysaccharide (sodium alginate, molecular weight $= 2.4 \times 10^6$ g/mol supplied by Sigma-Aldrich). The addition of alginate at 2, 4, 6, 8, 10, and 14 g/L produces six more aqueous phases. At 8, 10, and 14 g/L, the solutions present a low shear plateau and then a shear thinning behavior.

Because of the small gap, the average shear rate between the cylinders is constant within a few percent. We therefore use the continuous phases viscosities at $\dot{\gamma} = 990$ s^{-1}: $\eta_c = 11.8$, 24.3, 40.1, 66.5, 95.2, and 154.8 mPa s. Finally, we checked that none of the continuous phases present any measurable elasticity.

For each continuous phase, the experimental protocol previously described is realized to measure simultaneously the time evolution of the stress and the drop radius.

Results

Qualitative description of the emulsification process

Figure 3 summarizes typical measurements obtained in an emulsification experiment. The simultaneous evolution of the droplet size and the shear stress are displayed together with photographs of the emulsion at specific times. The confrontation of these data allows separating the emulsification process in different steps. In Figure 3a, the second photo from the left shows that at the end of the first step ($\sim$15 s), the two phases are still separated. As there is no noticeable mixing between the two phases, this step essentially corresponds to the development of the flow field. During this Step 1, the transport length is infinite, since the two phases are separated and transparent.

The first image allowing a measurement of the transport length, and therefore the determination of an average particle size, corresponds to the end of Step 2. In this second step a coarse emulsion (a premix) is formed.

Then, two different behaviors are observed. For sufficiently high continuous phase viscosities (see Figure 3a), there is a progressive reduction of the average droplet size with a simultaneous increase in shear stress, corresponding to Step 3. We call these "Type 1" emulsions, and this step "dynamical emulsification". Figure 3b shows that for a lower continuous phase viscosity, Step 3 is not observable. In this case, after Step 2, both the average particle size and the shear stress remain constant. We call these "Type 2" emulsions.

The third step for Type 1 emulsions is followed by a Step 4 where the properties of the emulsion are constant in time, both in terms of droplet size and shear stress. It is remarkable that the transition between Steps 3 and 4 is clearly marked: Figure 3a shows that there is an abrupt stop in both size reduction and shear stress increase. We call the characteristic time at the end of Step 3 the emulsification time t_e.

Experimental results

We have observed that the end of Step 2 occurs at an identical time around 90 s for all samples. Only one of the samples containing nonmodified dextran (at 29 mPa s) is of Type 1, whereas for alginate addition, all the samples are of Type 1 except for the lowest Alginate concentration (viscosity 11.8 mPa s). An important remark is that since the shear rate remains constant in time, when Step 3 occurs, an increase of shear stress also corresponds to an increase in the apparent viscosity of the emulsion.

In Table 1, a summary of the experimental findings is presented with the continuous phase viscosities, the initial and final droplet sizes and the emulsification time. For Type 2 emulsions, the size remains constant after the premix formation (end of Step 2, see Figure 3b). The data for one of the reproducibility experiments is presented for a continuous phase viscosity of 95.2 mPa s.

The Dynamical Emulsification Step

Experimental scaling

Figure 4 shows the shear stress measured during Step 3 versus the simultaneously determined average droplet radius for all Type 1 emulsions. Remarkably, the time parameter completely disappears in this representation, even though the measurements last typically for 3 h. The implicit time dependence, corresponding to a drop size decrease and a shear stress increase goes from the bottom right to the top left in Figure 4. In this representation, we observe that all experi-

Table 1. Summary of Results

Polymer	η_c (mPas)	R_{premix} (μm)	R_{final} (μm)	t_e (s)	Ca
Type 1					
Dextran	29	45.5	9.5	1100	0.25
Alginate	24.3	33	16.5	5500	0.33
Alginate	40.1	31.5	12	965	0.31
Alginate	66.5	32	11	440	0.34
Alginate	95.2	34.5	10	203	0.35
Alginate	95.2	33	8.5	200	0.29
Alginate	154.8	44.5	7.5	133	0.30
Type 2					
None	1.7	50	43	–	0.02
Dextran	6	28	27	–	0.07
Dextran	12	29	29	–	0.11
Dextran	20.6	32	30	–	0.14
Alginate	11.8	20.6	20	–	0.06

η_c is the continuous phase viscosity; R_{premix} corresponds to the first measurable transport length at the end of Step 2; R_{final} is the average size measured during Step 4; t_e: dynamical emulsification time determined at the end of Step 3 for Type 1 emulsions; Capillary number Ca is calculated from Eq. 3 with $R_{min} = 4.6$ μm.

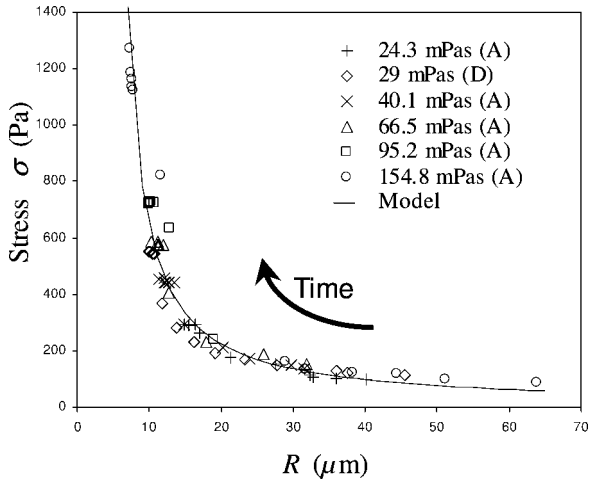

Figure 4. Measured shear stress vs. average particle size, during Step 3 for all Type 1 emulsions.

(A), Aliginate solutions; (D), Dextran solution. The model curve is Equation 2 with $A = 0.35$ and $R_{min} = 4.6$ μm.

mental points collapse onto a single curve for all the samples that present a dynamical emulsification (Type 1), whatever the viscosity of the continuous phase. In Figure 4, the shear stress is essentially inversely proportional to the average drop radius, showing that the instantaneous capillary number $\sigma(t)R(t)/\gamma$, remains nearly constant during the dynamical emulsification step.

Using the above observations, we use the simplest functional form that accounts correctly for the data:

$$\sigma(t) = \frac{A\gamma}{R(t) - R_{\min}}, \tag{2}$$

where A and R_{min} depend on the experimental set-up only (for a given surfactant and dispersed phase properties), and are in particular independent on the continuous phase viscosities, for both newtonian or non-newtonian samples. Adjustment of Eq. 2 to the experimental data points of Figure 4, using a standard least square method, leads to $A = 0.35$ and $R_{min} = 4.6$ μm.

The good agreement between Eq. 2 and the experimental data for all the continuous phase viscosities suggests that dynamical emulsification for shear experiments is fully driven by a constant capillary number of the following form:

$$\mathrm{Ca} = \frac{\sigma(R - R_{\min})}{\gamma} \tag{3}$$

Although experimentally deduced from Figure 4, the exact meaning of the minimum radius is not clear. Complementary experiments are needed to get a clear picture of its origin.

Emulsification occurrence: the critical capillary number

As shown above, the modified capillary number is constant during Step 3 for all continuous phase viscosities. Figure 5a shows these modified capillary numbers (defined by Eq. 3) as a function of the viscosity ratio for all the studied samples. In this figure, the modified capillary numbers are presented at the premix formation (end of Step 2) and in the final state (Step 4), showing that the modified capillary number remains constant in time during the whole experiment, whether dynamical emulsification occurs or not. For the experimental set-up considered here, dynamical emulsification only occurs if the modified capillary number at the end of Step 2 is close to a critical modified capillary number. This capillary number corresponds to the coefficient A in Eq. 2 and is experimentally found close to 0.35, in good agreement with Grace[5] ($0.5 < \mathrm{Ca_{cr}} < 1$) for a single droplet in the viscosity ratio studied here $0.02 < \eta_d/\eta_c < 2$.

A remarkable result of this work is that the concept of critical capillary number introduced for the break up condition of a single droplet also applies for the description of the whole dynamical shear induced emulsification process in

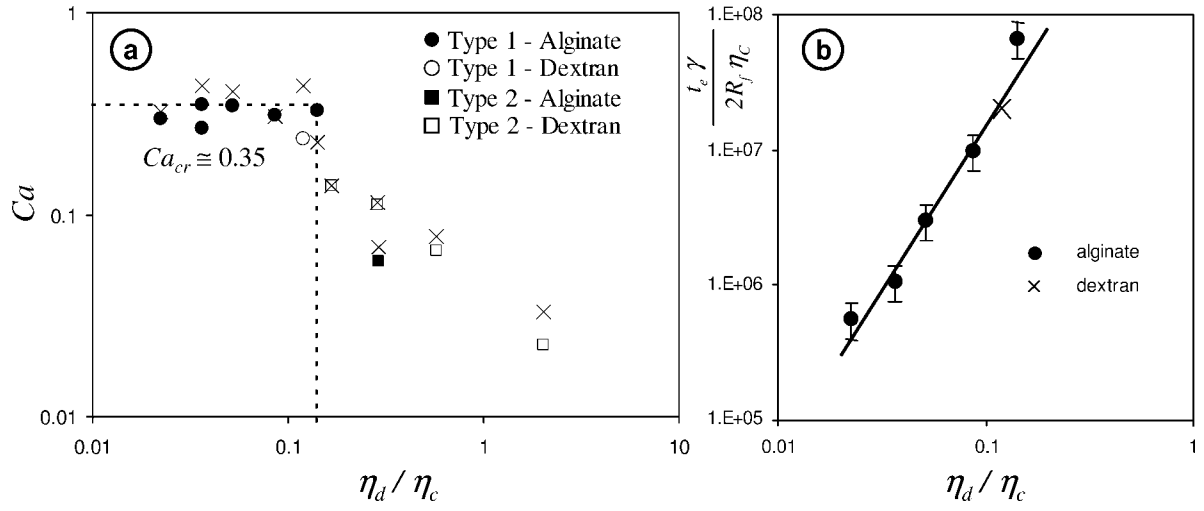

Figure 5. (a) Capillary number (from Table 1) vs. the viscosity ratio. Crosses and squares correspond to the capillary number at premix formation and during Step 4, respectively. (b) Dimensionless emulsification time vs. the viscosity ratio for Type 1 emulsions. The continuous line corresponds to a power law.

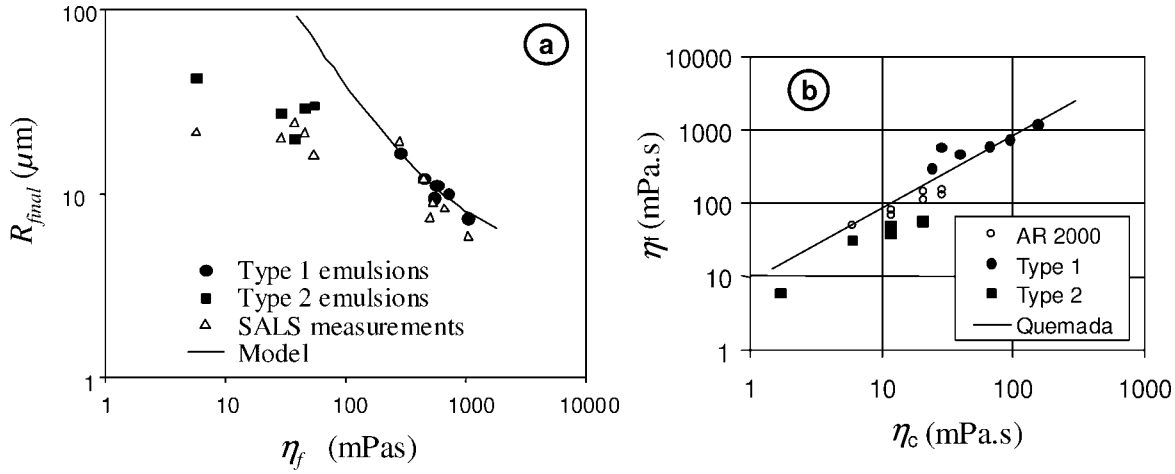

Figure 6. (a) Final average droplet radius; open triangles correspond to the average droplet radius in volume (Refs. 4,3) from the Malvern Mastersizer after strong dilution, and closed circles represent sizes determined with the optical apparatus at 50% in volume fraction; the solid line corresponds to the proposed model; (b) final viscosity of the emulsion vs. continuous phase viscosity.

AR 2000 data points are viscosity measurements performed after Step 4 with a cone and plate geometry (6 cm, 2°). The Quemada model is given by Eq. 4 with $\phi^* = 0.77$.

concentrated conditions. We nevertheless note that this capillary number, as written in Eq. 3, introduces a minimum radius, and uses the shear stress as the pertinent rheological variable.

Figure 5b shows, for Type 1 emulsions, the emulsification time divided by the critical deformation time of a single droplet $2R_{\text{final}}\eta_c/\gamma$ introduced by Grace.[5] This gives a dimensionless number much greater than unity, indicating that the time dependence of droplet break-up in concentrated regime involves a more complex mechanism than single droplet break up. The goal of the next paragraph is to understand why the emulsification process abruptly stops at the end of Step 3 for Type 1 emulsions.

Final State of Emulsions

Final average droplet radius

Figure 6a shows the final radius of droplets obtained for all samples by our technique, in good agreement with the volume-average particle size (R[4,3]) obtained by a Malvern Mastersizer X. Measurements made with the Mastersizer also show that all Type 2 emulsions have a comparable size distribution and that for Type 1 emulsions the polydispersity and average particle size decrease while increasing the continuous phase viscosity.

As mentioned previously, the apparent viscosity increases during Step 3 and stops at the end of this step. In Step 4, as there is no more droplet break-up, the energy supplied by the shear is essentially dissipated by the dispersion. So, since the complete process occurs at constant modified capillary number, the final droplet radius is, from Eq. 3: $R_{\text{final}} = R_{\min} + \text{Ca}_{\text{cr}}\gamma/(\eta_f\dot{\gamma})$ where η_f is the final emulsion viscosity (Step 4).

The average droplet radius for Type 2 emulsions is below the curve defined by Eq. 3 and corresponds to capillary numbers smaller than the critical capillary number. In our understanding, in the case of Type 2 emulsions, the viscous dissipation already dominates the elongation and break-up at the premix formation (Step 2), and explains why the dynamical emulsification cannot be observed.

Final emulsion viscosity

In the final state (Step 4), since break-up of droplets is absent, the emulsion viscosity reaches an upper limit that can be evaluated from hard sphere suspension models (neglecting the residual deformation of drops). For instance, using Quemada's model[16]:

$$\eta_f \cong \eta_c\left(1-\frac{\phi}{\phi^*}\right)^{-2}, \tag{4}$$

where ϕ is the volume fraction of particles (or droplets) and ϕ^* is the random packing fraction. Although the volume fraction of droplets is known (0.5 in this study), the close random packing fraction depends on the polydispersity of particles. For monodisperse rigid particles, this packing has been found close to 0.72,[17] but polydispersity is known to increase this value.[18] Figure 6b shows that reasonable agreement is obtained with $\phi^* = 0.77$. Using a constant value for the close random packing fraction is only an approximation since the polydispersity is not the same for all emulsions and residual deformation of droplets is neglected (see e.g. Ref. 19).

Conclusions

The dynamical emulsification process in concentrated systems (50% in volume) at constant applied shear rate is studied for various capillary numbers. Since the emulsions studied are highly turbid, the Steady Light Transport technique is used to follow dynamically the average particle size during the process. Simultaneously, the shear stress is measured

with a rheometer. We show that the time dependent process is divided into four steps:

- Step 1: Flow establishment in the shearing device.
- Step 2: Premix formation.
- Step 3: For capillary numbers greater than a critical capillary number of 0.35, a progressive size reduction of droplets, associated with an increase in shear stress.
- Step 4: A steady state when the emulsion properties remain constant, both in terms of droplet size and shear stress.

Focussing on Step 3, which we call dynamical emulsification, the simultaneous measurement of droplet size and shear stress shows that shear rate induced time dependent emulsification happens at constant critical capillary number defined as $Ca_{cr} = \sigma(t)(R(t) - R_{min})/\gamma$ where R_{min} and Ca_{cr} are expected to depend on the shearing device and the physicochemical properties of components, but can be experimentally obtained with the present experimental setup. The definition of this capillary number is independent on the continuous phase viscosity or its newtonian or non-newtonian nature. Thus, an a priori general relationship is obtained between the shear stress and the average drop size during emulsification, which allows prediction of the final average droplets size. This process ends when the viscosity increase during dynamical emulsification reaches its maximum value corresponding to a viscous dissipation associated to hydrodynamic interactions between droplets.

These understandings of emulsification mechanism in concentrated conditions might be helpful for optimization of emulsion formulation.

Acknowledgments

We would like to thank Alan Parker, from Firmenich SA for useful comments and discussions.

Literature Cited

1. Shervin CR, Raughley DA, Romaszewski RA. Flow visualization scalup studies for the mixing of viscoelastic fluids. *Chem Eng Sci*. 1991;46:2867–2873.
2. Aronson MP, Petko MF. Highly concentrated water-in-oil emulsions: influence of electrolyte on their properties and stability. *J Colloid Interf Sci*. 1993;159:134–149.
3. Sanchez MC, Berjano M, Guerrero A, Brito E, Gallegos C. Evolution of the microstructure and rheology of o/w emulsions process. *Canadian J Chem Eng*. 1998;76:479–485.
4. Taylor GI. The formation of emulsions in definable fields of flow. *Proc R Soc London A*. 1934;146:501–523.
5. Grace HP. Dispersion phenomena in high viscosity immiscible fluid systems and application of static mixers as dispersion devices in such systems. *Chem Eng Commun*. 1982;14:225–277.
6. Mabille C, Leal-Calderon F, Bibette J, Schmitt V. Monodisperse fragmentation in emulsions: mechanisms and kinetics. *Europhys Lett*. 2003;61:708–714.
7. Baravian C, Caton F, Dillet J, Mougel J. Steady light transport under flow: characterisation of evolving dense random media. *Phys Rev E*. 2005;71:066603.
8. Baravian C, Lalante A, Parker A. Vane rheometry with a large, finite gap. *Appl Rheol*. 2002;12:81–87.
9. Baravian C, Caton F, Dillet J. Steady light diffusion application to rheology: a new tool for the characterization of concentrated suspensions. *Rheol Acta*. 2004;43:427–432.
10. Mougel J, Alvarez O, Baravian C, Caton F, Marchal P, Stébé MJ, Choplin L. Aging of an unstable w/o gel emulsion with a nonionic surfactant. *Rheol Acta*. 2006;45:555–560.
11. Haskell RC, Svaasand LO, Tsay TT, Feng TC, McAdams MS, Tromberg BJ. Boundary conditions for the diffusion equation in radiative transfer. *J Opt Soc Am A*. 1994;11:2727–2741.
12. Kienle A, Patterson MS. Improved solutions of the steady state and the time-resolved diffusion equations for reflectance from semi-infinite turbid medium. *J Opt Soc Am A*. 1997;14:246–254.
13. Caton F, Baravian C, Mougel J. The influence of the microscopic characteristics of a random medium on incoherent light transport. *Opt Express*. 2007;15:2847–2872.
14. Rouzès C, Durand A, Léonard M, Dellacherie E. Surface activity and emulsification properties of hydrophobically modified dextrans. *J Colloid Interf Sci*. 2002;253:217–223.
15. Rotureau E, Léonard M, Marie E, Dellacherie E, Camesano T, Durand A. From polymeric surfactants to colloidal systems (1): Amphiphilic dextrans for emulsion preparation. *Colloids Surf A*. 2006;288:131–137.
16. Quemada D. Rheology of concentrated disperse systems and minimum energy dissipation principle, Part 1. Viscosity-concentration relationship. *Rheol Acta*. 1977;16:82–94.
17. Jones DA, Leary B, Boger DV. The rheology of concentrated colloidal suspension of hard spheres. *J Colloid Interf Sci*. 1991;147:479–495.
18. Ouchiyama N, Tanaka T. Porosity estimation for random packings of spherical particles. *Ind Eng Fundam*. 1984;23:490–493.
19. Mills P, Snabre P. Rheology of weakly flocculated suspensions of viscoelastic particles. *J Phys III France*. 1996;6:1835–1855.

Manuscript received Feb. 5, 2007, and revision received May 5, 2007.